This is the peer-reviewed, final accepted version for American Mineralogist, published by the Mineralogical Society of America.
The published version is subject to change. Cite as Authors (Year) Title. American Mineralogist, in press.
DOI: https://doi.org/10.2138/am-2022-8112. http://www.minsocam.org/

REVISION I

Uranotungstite, the only natural uranyl tungstate: crystal structure revealed from 3D electron diffraction

GWLADYS STECIUK[1], UWE KOLITSCH[2,3], VIKTOR GOLIÁŠ[4], RADEK ŠKODA[5], JAKUB PLÁŠIL[1§] AND FRANZ XAVER SCHMIDT[6]

[1] Institute of Physics ASCR, v.v.i., Na Slovance 1999/2, 18221 Prague 8, Czech Republic

[2] Mineralogisch-Petrographische Abt., Naturhistorisches Museum, Burgring 7, 1010 Wien, Austria

[3] Institut für Mineralogie und Kristallographie, Universität Wien, Althanstraße 14, 1090 Wien, Austria

[4] Institute of Geochemistry, Mineralogy and Mineral Resources, Faculty of Science, Charles University in Prague, Albertov 6, CZ–128 43, Prague 2, Czech Republic

[5] Department of Geological Sciences, Faculty of Science, Masaryk University, Kotlářská 2, 611 37, Brno, Czech Republic

[6] Staatliches Museum für Naturkunde Stuttgart, Rosenstein 1, 70191 Germany

ABSTRACT

Uranotungstite is an uranyl-tungstate mineral that was until recently only partially characterized with a formula originally given as $(Fe^{2+},Ba,Pb)(UO_2)_2(WO_4)(OH)_4 \cdot 12H_2O$ and an unknown crystal structure. This mineral has been reinvestigated by electron microprobe analysis coupled with 3D electron diffraction. According to the electron microprobe data, the holotype material from the Menzenschwand uranium deposit (Black Forest, Germany) has the empirical formula $(Ba_{0.35}Pb_{0.27})_{\Sigma 0.62}[(U^{6+}O_2)_2(W^{6+}_{0.98}Fe^{3+}_{0.26}\square_{0.75})O_{4.7}(OH)_{2.5}(H_2O)_{1.75}](H_2O)_{1.67}$ (average of 8 points

§ Email: plasil@fzu.cz

Always consult and cite the final, published document. See http:/www.minsocam.org or GeoscienceWorld

This is the peer-reviewed, final accepted version for American Mineralogist, published by the Mineralogical Society of America.
The published version is subject to change. Cite as Authors (Year) Title. American Mineralogist, in press.
DOI: https://doi.org/10.2138/am-2022-8112. http://www.minsocam.org/

calculated on the basis of 2 U *apfu*; the H_2O content derived from the structure). According to the precession-assisted 3D ED data, holotype uranotungstite from Menzenschwand is monoclinic, $P2_1/m$, with a = 6.318(5) Å, b = 7.388(9) Å, c = 13.71(4) Å, β = 99.04(13)° and V = 632(2) Å^3 (Z = 2). The structure refinement of the 3D ED data using the dynamical approach (R_{obs} = 0.0846 for 3287 independent observed reflections) provided a structure model composed of heteropolyhedral sheets. A β-U_3O_8-type sheet of idealized composition $[(UO_2)_2W^{6+}Fe_{0.25}{}^{3+}\square_{0.75}O_{4.75}(OH)_{1.5}(H_2O)_{1.75}]^{0.25-}$ is composed of UO_7 polyhedra linked by $(W,Fe)O_5$ polyhedra in which the W:Fe ratio is variable as well as the bulk occupancy of this site; the W site may also host a minor proportion of Cu, Mg, or V. In uranotungstite, the interlayer spaces between adjacent U-W-O sheets host water on one side and, on the other side, a partially occupied cation site mostly occupied by Ba and, to a lesser extent, Pb, as well as a partially occupied H_2O site. This work is the first structural description of a natural uranyl-tungstate mineral and confirms the great structural and chemical flexibility of β-U_3O_8 type of sheets.

Keywords: uranotungstite, uranyl tungstate, crystal structure, crystal chemistry, Menzenschwand, 3D electron diffraction.

INTRODUCTION

Uranotungstite is the only uranyl tungstate known in nature and is a scarce alteration product of oxidation-hydration weathering of uraninite. Its rarity mostly arises from a rather unusual association of uranium and tungsten in the most common types of uranium deposits worldwide. It was described for the first time by Walenta (1985) from the Menzenschwand (also referred to as Krunkelbach) uranium deposit in the Black Forest, Baden-Württemberg, Germany. The type

Always consult and cite the final, published document. See http:/www.minsocam.org or GeoscienceWorld

material forms spherulitic aggregates of 0.3 mm in diameter and is associated with meta-uranocircite, meta-heinrichite, and other secondary uranium minerals. Apart from the commonly observed yellow, brown-yellow to orange colors, the mineral may also be olive-green, greenish, or blackish. Electron microprobe analysis (EMPA) of the type material led to the reported empirical formula $(Fe_{0.38}Ba_{0.37}Pb_{0.36})_{\Sigma 1.11}U_{1.82}W_{0.99}H_{28.94}O_{24}$, where Fe was considered divalent. This formula was then idealized to (Fe, Ba, Pb)$(UO_2)_2(WO_4)(OH)_4 \cdot 12H_2O$ by Walenta (1985). Later on, more uranotungstite was found by Walenta (1985) from the Clara barite-fluorite mine in the Black Forest, Germany, but in the Clara mine material, only traces of Ba and no Pb were semiquantitatively detected.

Based on the morphology of the lath-like crystals of the type material, the mineral was first assumed to be orthorhombic and the unit-cell parameters a = 9.22, b = 13.81, c = 7.17 Å (Z = 2) were proposed on the basis of a tentatively indexed X-ray powder diffraction pattern. The lath-like crystals show (010) as a flattening plane and they exhibit perfect cleavage. Unlike the type material from Menzenschwand, the Clara mine samples rather show thin platy, subparallel crystals with a diamond-shaped outline. Nevertheless, the crystal structure of the type material could not be determined by X-ray diffraction (powder or single crystal) due to the very small size and subparallel intergrowth of the crystals. More generally, except for its original description, the mineral has remained poorly studied; the crystal structure was still unknown before our present study and there is not much available information about the crystal chemistry and the paragenetic position in the weathering process. Furthermore, some aspects of the original description appeared to be doubtful: (i) the presence of Fe^{2+} in a mineral formed under oxidizing conditions; (ii) the co-assignment of Fe, Ba, and Pb in the chemical formula. We point out that previous studies show that Fe^{3+} and W^{6+} replace each other in the crystal structures of oxide minerals

Always consult and cite the final, published document. See http:/www.minsocam.org or GeoscienceWorld

because of their very similar ionic radii (Kolitsch 1998; Atencio et al. 2010). Moreover, as demonstrated by microchemical tests of a Clara mine sample using the reagents Merckoquant 10.004 (Fa. Merck) and KSCN, the iron in the mineral is trivalent, not divalent as it was suggested in the early studies. Among the large cations, either Ba^{2+}, Pb^{2+}, K^{+}, or Bi^{3+} may be dominant (the latter two are not present in the type material) and minor or trace contents of Cu are very common. In some samples associated with lenoblite, $V_2^{4+}O_4 \cdot 2H_2O$, notable amounts of V, up to ~4 at. %, were found, as well as trace amounts of Mg. Another example of the chemical variety existing in uranotungstite is illustrated by an uranotungstite sample from Les Montmins, Allier, France, for which Cuchet et al. (2000) reported Pb, U, W, and Fe as well as trace amounts of Ba, P, Cu, and As.

All the above-mentioned facts motivated us to reinvestigate uranotungstite from the type locality (Menzenschwand) by EMPA and the entire suite of uranotungstite-like phases from elsewhere. The attempted structural study of specimens from Menzenschwand was severely hampered by the fact that uranotungstite does not form crystals large enough to be used by conventional X-ray diffraction methods. Nevertheless, in the light of the recent success and developments of 3D electron diffraction techniques (3D ED) (Gemmi and Lanza 2019; Gemmi et al. 2019) such a study is now possible and was undertaken on uranotungstite from the type locality. Here we present the first crystal-structure determination of this unique natural uranyl tungstate mineral.

SPECIMENS AND OCCURRENCES

The two samples used in this study originate from the Menzenschwand uranium deposit, Black Forest (Schwarzwald), Germany, which is the type locality for uranotungstite (Walenta 1985).

Always consult and cite the final, published document. See http:/www.minsocam.org or GeoscienceWorld

This is the peer-reviewed, final accepted version for American Mineralogist, published by the Mineralogical Society of America.
The published version is subject to change. Cite as Authors (Year) Title. American Mineralogist, in press.
DOI: https://doi.org/10.2138/am-2022-8112. http://www.minsocam.org/

We used the holotype specimen of uranotungstite deposited in the collection of the Staatliches Museum für Naturkunde in Stuttgart (Germany). Due to a minimal volume available for the analysis, the sample from the holotype specimen was prepared for the polished-section mount directly in the museum and used for subsequent EMPA (sample 1). The holotype specimen consists of a quartz-barite gangue with disseminated to massive supergene uranyl minerals. Besides uranotungstite, they comprise uranocircite/metauranocircite and most probably meta-heinrichite, mentioned in the original description. Visual inspection suggests that there are at least two types of tabular crystals belonging probably to different minerals of the so-called uranium micas. Uranotungstite forms small orange spherules, consisting of fine tabular crystals; these spherules reach up to 0.3–0.4 mm across.

Additionally, a rich specimen of uranotungstite from Menzenschwand obtained via Carsten Slotta (Mintreasure.com, Hausach, Germany) has been used for the 3D ED characterization (sample 2) (Fig. 1). Uranotungstite forms globular to massive aggregates of orange color in vugs of a quartz gangue with relics of uraninite (scarce). Along with rare uranotungstite, the vugs host uranophane, studtite, phosphuranylite, billietite, and ubiquitous hematite. Surprisingly, later on, during the transmission electron microscopy experiments, it was found that the orange crystalline aggregates studied consist of uranotungstite, but the prevailing phase is francevillite, which has not been reported from Menzenschwand so far.

Apart from the specimens mentioned above, we also investigated several uranotungstite-like phases from the Clara mine (Germany) and the Medvědín uranium deposit (Czech Republic), but only the latter will be addressed here.

CHEMICAL COMPOSITION

Always consult and cite the final, published document. See http:/www.minsocam.org or GeoscienceWorld

This is the peer-reviewed, final accepted version for American Mineralogist, published by the Mineralogical Society of America.
The published version is subject to change. Cite as Authors (Year) Title. American Mineralogist, in press.
DOI: https://doi.org/10.2138/am-2022-8112. http://www.minsocam.org/

The chemical composition of the very small sample extracted from the holotype specimen (sample 1) was determined quantitatively using a Cameca SX100 electron microprobe operating in wavelength-dispersive mode (WDS) and operated with an accelerating voltage of 15 kV, a beam current of 4 nA, and a 5 μm beam diameter. All samples were stable under the beam. The following X-ray lines and standards and lines were used: Ca *K*α (wollastonite), K *K*α (sanidine), Fe *K*α (andradite), W *L*α ($ZnWO_4$), Ba *L*β ($BaSO_4$), Pb *M*α (vanadinite), and U *M*α (parsonsite). The elements F, Na, Mg, Al, Si, P, S, Cl, Ti, V As, Se, Sr, and Bi were also sought, but their contents were below the respective detection limits. The peak counting times were 10–20 s, and the counting time for each background point was 50% of the time for the peak. The measured intensities were converted to elemental concentrations using the PAP program (Pouchou and Pichoir 1985). The type material from Menzenschwand (Table 1) has the following empirical formula (average of eight points, calculations based upon 2 U atoms per formula unit, *apfu*): $(Ba_{0.35}Pb_{0.27})_{\Sigma 0.62}[(U^{6+}O_2)_2(W^{6+}_{0.98}Fe^{3+}_{0.26}\square_{0.75})O_{4.7}(OH)_{2.5}(H_2O)_{1.75}](H_2O)_{1.67}$ (the proportions of O and OH were obtained from the stoichiometry derived from the structure refinement, see section Discussion for details). The cation stoichiometry of this formula is, except for H and O associated with OH/H_2O, reasonably close to the one determined by Walenta (1985), $(Fe_{0.38}Ba_{0.37}Pb_{0.36})_{\Sigma 1.11}U_{1.82}W_{0.99}H_{28.94}O_{24}$.

The chemical composition of the uranotungstite used for the structure determination was determined only semiqualitatively using an EDS detector coupled to the transmission electron microscope used for precession electron diffraction tomography. The semiquantitative elemental ratios obtained from the EDS spectra (Fig. 2) are Ba:Pb ~ 80:20 and W:Fe ~ 53:47.

3D ELECTRON DIFFRACTION AND STRUCTURE DETERMINATION

Always consult and cite the final, published document. See http:/www.minsocam.org or GeoscienceWorld

This is the peer-reviewed, final accepted version for American Mineralogist, published by the Mineralogical Society of America.
The published version is subject to change. Cite as Authors (Year) Title. American Mineralogist, in press.
DOI: https://doi.org/10.2138/am-2022-8112. http://www.minsocam.org/

3D ED data collection

Transmission electron microscopy (TEM) has been chosen for the structural characterization of uranotungstite due to the limited amount of available material, the minute size of uranotungstite crystals, and the concomitant presence of francevillite (Fig. 3). A few pieces of the mineral were scratched from the Menzenschwand sample 2 and gently crushed in ethanol. A drop of the uranotungstite-containing ethanol was then deposited on a Cu-grid covered with a thin film of holey amorphous carbon. To preserve the hydrated nature of uranotungstite under the high TEM vacuum, the cryo-plunging conditions were used to transfer the sample in the TEM: the grid was plunged into liquid nitrogen and then transferred to an FEI Tecnai 02 TEM (acceleration voltage of 200 kV, LaB_6) using a Gatan cryo-transfer holder and equipped with a side-mounted CCD camera Olympus Veleta with a 14-bit dynamic range. This method, initially used for organic and biological samples, was recently applied to hydrated inorganic samples (Mugnaioli et al. 2020; Steciuk et al. 2019, 2021) and is now used routinely in our group to analyze new minerals by 3D ED. Nowadays, single-crystal electron diffraction data can be collected using one of the 3D ED techniques that are extensively described in Gemmi and Lanza (2019) and Gemmi and Mugnaioli (2019). In this study, the precession-assisted electron diffraction tomography (PEDT) method was used (Vincent and Midgley 1994; Kolb et al. 2007, 2008; Mugnaioli et al. 2009) wherein the precession of the electron beam aims to reduce the dynamic effects. The precession angle of the beam was kept at 1° during the experiment using the precession device Nanomegas Digistar. Finding a good candidate to collect 3D ED data on uranotungstite was a challenging task as the majority of crystals barely diffract. A lower crystallinity of the supergene minerals, to which uranotungstite belongs, is commonly observed, and diffraction data often suffer from disorder features and low resolution (Steciuk et al. 2020). Small diffracting crystal fragments were

Always consult and cite the final, published document. See http:/www.minsocam.org or GeoscienceWorld

fortunately found at the nanoscale, partially covered by francevillite (Fig. 3), from which PEDT data could be recorded at 100 K. For each selected crystal area, a series of non-oriented patterns are sequentially collected by step of 1° on the accessible tilt range of the goniometer automated by the in-house software, including the tracking of the crystal following the procedure described by Plana-Ruiz et al. (2020) and Kolb et al. (2019). The data reduction was performed using the computer programs PETS2 (Palatinus et al. 2019).

Data processing and structure solution

Based on two merged data sets, uranotungstite is monoclinic, a = 6.318(5) Å, b = 7.388(9) Å, c = 13.71(4) Å, β = 99.04(13)° and V = 632(2) Å^3. The reciprocal-space sections are consistent with the space group $P2_1/m$ (with the extinction condition k = 2n for 0k0 reflections) (Fig. 3). This unit cell and space group provide very satisfactory indexing of the X-ray powder diffraction pattern reported by Walenta (1985). New features in PETS2 allow a better data reduction of 3D ED data by optimizing the orientation and the scale of each frame and fitting the intensity profile for the integration (for detailed information, check Palatinus et al. 2019). This procedure leads to two *hkl*-type files: one for the structure solution and the kinematical refinement (where the two data sets are combined), and another file (one for each data set) dedicated to the dynamical refinement where each ED frame is considered independent (Palatinus et al. 2015a, b). The completeness reached 83.6% for a sinθ/λ = 0.7 Å^{-1} resolution shell (Tab. 4). The structure was solved with the Superflip program (Palatinus and Chapuis 2007; Palatinus 2013) and refined from 3D ED data using Jana2020 (Petříček et al. 2014).

The initial structure model showed a layered structure where the electrostatic potential map defined a rather sharp and fully occupied uranyl-MO$_5$ layer (M = W^{6+} and Fe^{3+}) and two types of

Always consult and cite the final, published document. See http:/www.minsocam.org or GeoscienceWorld

interlayers: one containing a partially occupied Ba/Pb position surrounded by water molecules, and another one with a water molecule only. The single *M* site is shared by W^{VI} and Fe^{III}. To stabilize the refinement of the partially occupied Ba/Pb site, the Ba:Pb ratio was set to 80:20 according to the ratio obtained by energy-dispersive spectroscopy (EDS) coupled to the TEM. The EDS analysis also shows a Fe:W ratio around 53:47 but this value is possibly inaccurate and the proper ratio is better determined from the refinement of the fully occupied Fe/W site. Restraints were applied in the refinement of 3D ED data because the lack of coverage along **c** is responsible for a lower accuracy of the *z/c* coordinates. The bond distances among the U sites and the apical oxygen atoms constituting the UO_2^{2+} ion were restrained to a value of 1.800(2) Å (Evans 1963; Burns et al. 1997a; Lussier et al. 2016). Additionally, a soft restraint of 1.920(3) Å was applied to the bond length between W1 and its apical oxygen ligand (O5). Moreover, the overall occupancy of Ba and Pb must, at least, compensate for the additional negative charge occurring when Fe^{3+} substitutes W^{6+} and was thus restricted accordingly (conformation C in Fig. 4). Note that the free refinement gives a slightly lower value for the cumulative occupancy of Ba and Pb, showing that the conformation labeled B in Figure 4 is improbable in the two studied crystal fragments. Two hydrogen positions around O3 were weakly revealed by the difference potential map after few refinement steps (Palatinus et al. 2017). The small proportion of hydrogen linked to O5 (H_2O) when Fe is located in the octahedrally coordinated site is not visible from our data. The O–H distances were restrained to 1.000(2) Å with the isotropic displacement parameters of the hydrogen atoms set as riding with an extension factor of 1.5. The final refinement converged to R_{obs}/wR_{obs} = 0.0846/0.0589 for 3287 independent observed reflections, with $I > 3\sigma(I)$. With a refined occupancy of $W_{1.20(1)}Fe_{0.80(1)}$ the structural formula is $(Ba_{0.32}Pb_{0.08})_{\Sigma 0.40}[(U^{6+}O_2)_2W^{6+}_{1.2}Fe^{3+}_{0.8}O_{7.2}(H_2O)_{3.2}]$ for $Z = 2$. The complete CIF file, also

Always consult and cite the final, published document. See http:/www.minsocam.org or GeoscienceWorld

This is the peer-reviewed, final accepted version for American Mineralogist, published by the Mineralogical Society of America.
The published version is subject to change. Cite as Authors (Year) Title. American Mineralogist, in press.
DOI: https://doi.org/10.2138/am-2022-8112. http://www.minsocam.org/

containing a block with the full reflection data, is deposited as Supplemental material. Selected interatomic distances are reported in Table 2, the full bond-valence analysis (following general rules given by Brown 1981, 2002, and using bond-valence parameters from Gagné and Hawthorne 2015) is provided as Supplementary Table S1.

DESCRIPTION OF THE STRUCTURE

The structure of uranotungstite contains fifteen independent atom sites (non-hydrogen) in the asymmetric unit. There are two unique U sites; one unique mixed (W,Fe) site; one partially occupied, interlayer (Ba,Pb) mixed site, and eleven O sites of which two (labeled O3 and O10) correspond to interlayer H_2O/OH groups (Fig. 4). The U sites are coordinated by seven O atoms; two of them (further designated as O_{Ur}) represent strongly bonded atoms in the UO_2^{2+} ion at a distance of ~1.8 Å from the central U atom (Evans 1963; Burns et al. 1997a; Lussier et al. 2016). The other five atoms of the UO_7 polyhedra are localized at the horizontal apices of the pentagonal bipyramid. The mixed (W,Fe) site is coordinated by five ligands up to 2 Å in the form of a tetragonal pyramid. The (Ba,Pb) site is coordinated to eight ligands (up to 3 Å), including two O_{Ur} atoms (O6 and O8), the apical O atom of the (W,Fe)-polyhedra (symmetrically related O5), and H_2O groups (O10 in the (010) plane) (Tables 2, S1).

The UO_7 polyhedra share edges to form infinite chains of polyhedra extending along [010] that are interconnected *via* $(W,Fe)O_5$ polyhedra (Fig. 5). The uranyl-anion topology of the uranotungstite sheet is shown in Fig. 4b. This sheet is built from pentagons, squares, and triangles; pentagons and squares are centered by U^{VI} and (W,Fe), while the centers of triangles are not occupied in uranotungstite. The sheet topologically belongs to that of the β-U_3O_8 type, which is characterized by the sequence …**DRU**… (Fig. 5c) (Miller et al. 1996; Burns 2005).

Always consult and cite the final, published document. See http:/www.minsocam.org or GeoscienceWorld

This is the peer-reviewed, final accepted version for American Mineralogist, published by the Mineralogical Society of America.
The published version is subject to change. Cite as Authors (Year) Title. American Mineralogist, in press.
DOI: https://doi.org/10.2138/am-2022-8112. http://www.minsocam.org/

Additionally, apart from the structure of β-U_3O_8 (Loopstra 1970), such a sheet was also found in the structures of ianthinite (Burns et al. 1997), billietite (Finch et al. 2006), spriggite (Brugger et al. 2006), rameauite (Plášil et al. 2016), shinkolobweite (Olds et al. 2017), and nollmotzite (Plášil et al. 2018). The stacking of the U-(W,Fe)-O sheets parallel to (001) is based on the alternation of U-(W,Fe)-O sheets of 3.94 Å thickness with, on one side, a layer occupied only by water molecules (O3) (layer thickness 2.14 Å) and, on the other side, a layer containing a (Ba,Pb) site and an H_2O (O10) molecule with a layer thickness of 3.49 Å (Fig. 6). In this way, the unit cell has a general stacking sequence built from four layers: U-(W,Fe)-O sheet | H_2O/OH | U-(W,Fe)-O sheet | (Ba,Pb)–H_2O. The layered character of the uranotungstite structure explains the perfect cleavage of the mineral parallel to (001) and its platy crystal habit.

DISCUSSION

The chemical formula of uranotungstite

The chemical formula of uranotungstite is interesting in many ways as all the reported analyzed specimens of uranotungstite exhibit a wide compositional diversity. This is evident in the type material found in the Menzenschwand deposit with a high amount of W Pb, Ba, and Fe, to specimens with only traces of Pb and Ba from the Clara mine and others, containing additional traces of several other elements like V, Mg, or Cu. Another example comes from the aforementioned uranotungstite from Les Montmins in France that is Pb-dominant, with only traces of Ba, Cu, P, and As (Cuchet et al. 2000). From 3D ED data collected at the nanoscale from Menzenschwand sample 2, the (W,Fe) site $(W_{1.2}Fe_{0.8})_{\Sigma 2}$ appears fully occupied, unlike what is shown by the EPMA data (sample 1) at a larger scale with $(W_{0.98}Fe_{0.26})_{\Sigma 1.24}$. In uranotungstite, the cationic disorder and the vacancies in the Ba/Pb and W/Fe sites offer four theoretically

Always consult and cite the final, published document. See http:/www.minsocam.org or GeoscienceWorld

possible local conformations labeled A, B, C, and D where the amount of water molecules and/or hydroxyl groups is variable (Fig. 4); in the following discussion, x is the number of OH+H_2O visible in the refined model, and n is the theoretical number of additional water molecules in the interlayer. While those conformations are only representing local ordering schemes and end-members, they allow a better understanding of the significant chemical variability observed between the two studied samples first, and, to a larger extent, in uranotungstite samples from different localities. The two theoretical conformations A and D are defined as the two end-members with formulas $(UO_2)_2W_2O_8(H_2O)_2$ and $(UO_2)_2(OH)_4(H_2O)_6$. They are considered as end-members as they both exhibit an empty interlayer in the absence of (Ba, Pb) and its associated H_2O (O10). In conformation B, the presence of Ba and W gives a formula $(Ba,Pb)(UO_2)_2W_2O_8(OH)_2(H_2O)$ that promotes a hydroxyl group allowing three H_2O/OH (x = 3). On the other hand, the presence of Fe^{III} in the W/Fe (conformation C) site brings three additional negative charges, and the concomitant presence of Ba/Pb is a necessary condition to enable charge neutrality, leading to an ideal hypothetical W-free composition of $(Ba,Pb)(UO_2)_2Fe_2O_6(H_2O)_5$ (x = 5). In conformations B and C the stacking of the layers is stabilized by covalent and strong hydrogen bonds and there is no obvious spare space to host additional interlayer water molecules (n) (Fig. 4a). However, from our structural model, in the two end-members A (x = 2) and D (x = 10), the stacking of the U-W/Fe layers is ensured by strong hydrogen bonds on one side whereas, on the other side, the empty interlayer (Ba,Pb,H_2O) has to be filled by additional interlayer H_2O molecules to allow the layers to be connected. In theory, for each conformation A and D (for Z = 2), the interlayer can host at least n = 2 additional H_2O (Fig. 4b). Results of the 3D ED data show 60% and 40% of the conformations A and C, respectively. The refinement shows clearly that the B conformation is not significantly present as

Always consult and cite the final, published document. See http:/www.minsocam.org or GeoscienceWorld

This is the peer-reviewed, final accepted version for American Mineralogist, published by the Mineralogical Society of America.
The published version is subject to change. Cite as Authors (Year) Title. American Mineralogist, in press.
DOI: https://doi.org/10.2138/am-2022-8112. http://www.minsocam.org/

the amount of (Ba,Pb), when freely refined, barely compensates the negative charge brought by the presence of Fe^{III} (conformation C) on the (W,Fe) site and was later restricted to ensure charge balance. It means that there is not enough (Ba,Pb) to allow conformation B to occur in the two crystals used for the structural analysis. On the other hand, the EMPA data of sample 1, which were measured at a larger scale, document the presence of 49% of conformation B, 13% of C, and 38% of D (Fig. 4). Therefore, two uranotungstite compositions are determined: EMPA of sample 1 gives a formula $(Ba_{0.35}Pb_{0.27})_{\Sigma 0.62}[(U^{VI}O_2)_2(W^{VI}_{0.98}Fe^{III}_{0.26}\square_{0.75})O_{4.7}(OH)_{2.5}(H_2O)_{1.75}]$-$(H_2O)_{1.67}$, whereas 3D ED and TEM-EDS of sample 2, distinctly poorer in Pb, but richer in Fe, leads to $(Ba_{0.32}Pb_{0.08})_{\Sigma 0.40}[(U^{VI}O_2)_2W^{VI}_{1.2}Fe^{III}_{0.8}O_{7.2}(H_2O)_{1.75}](H_2O)_{1.45}$. Considering the possible additional water molecules allowed by the conformations A and D, the 3D ED model contains from $x = 3.2$ to $x + n \approx 4.4$ water molecules while the EMPA data correspond to a range from $x = 5.9$ to $x + n \approx 6.7$ molecules.

Using the same structural model, the compositions differ by their proportions of Ba/Pb and W/Fe as well as for the bulk occupancies of these two cationic sites. However, Ba and W always remain dominant over Pb and Fe, and no other elements are detected. In that regard, the cation proportions are in line with the compositional characteristics of the type material. The difference between the formula derived by EPMA and the refinement of 3D ED data is easily explained by the possible local variation of the samples' compositions. Our 3D ED study is based on the two best-crystallized areas found during the experiment and might not represent uranotungstite's bulk composition. It demonstrates that the structure of uranotungstite allows and is characterized by a significant chemical variability. Because the EPMA data are more representative of the bulk composition, the ideal formula of uranotungstite is set accordingly as $(Ba_{0.35}Pb_{0.27})_{\Sigma 0.62}[(U^{VI}O_2)_2(W^{VI}_{0.99}Fe^{III}_{0.26}\square_{0.75})O_{4.75}(OH)_{1.5}(H_2O)_{1.75}](H_2O)_{1.67}$. From this formula,

Always consult and cite the final, published document. See http:/www.minsocam.org or GeoscienceWorld

This is the peer-reviewed, final accepted version for American Mineralogist, published by the Mineralogical Society of America.
The published version is subject to change. Cite as Authors (Year) Title. American Mineralogist, in press.
DOI: https://doi.org/10.2138/am-2022-8112. http://www.minsocam.org/

the ideal composition of the U-W/Fe-O sheet shown in Fig. 6 becomes $[(UO_2)_2(WFe_{0.25}\square_{0.75})O_{4.75}(OH)_{1.5}(H_2O)_{1.75}]^{0.25-}$, with two interlayers $[(Ba_{0.354}Pb_{0.271})_{\Sigma 0.625}(H_2O)_{0.625}]^{1.25+}$ and $[(H_2O)(OH)]^{-}$.

The chemical formula obtained from the results of the crystal-structure refinement and EPMA is not consistent with the formula given by Walenta (1985) in the original description. First, it is unambiguous that Fe^{III} partially occupies the W^{VI} site and does not exist as isolated cations in the interlayer space; only Ba^{2+}/Pb^{2+} cations and H_2O molecules are localized there. Furthermore, it is clear that the simplified formula given by Walenta (1985), $(Fe^{II},Ba,Pb)(UO_2)_2(WO_4)(OH)_4 \cdot 12H_2O$, as well as the current IMA-accepted formula, $Fe(UO_2)_2(WO_4)(OH)_4 \cdot 12H_2O$, both differ from the presently obtained formula, namely in the overall H_2O content (considered as H_2O + OH). While these formulae contain 14 H_2O in total, our results indicate a much lower content, up to about 6 H_2O molecules per formula unit (OH + H_2O). Adding the theoretical *n* H_2O to the formula brings the number up to 7, still far from the 14 H_2O of Walenta (1985). The H_2O content given by Walenta (1985) was determined by calculations of the weight loss after heating a sample up to 350 °C, however, without any details given. According to Walenta (1985), the electron microprobe analyses were then recalculated, including the corresponding weight (in wt. %) of H_2O obtained from the heating. Since there are no details in the paper by Walenta (1985) we cannot exclude that the sample was contaminated and we should consider these results with caution.

The newly undertaken chemical analysis of uranotungstite holotype material nonetheless documented that the cation content of the formula given initially by Walenta (1985) is not so far from that determined here. The redetermined composition of the holotype uranotungstite from Menzenschwand by EPMA, $(Ba_{0.35}Pb_{0.27})_{\Sigma 0.62}[(U^{VI}O_2)_2(W^{VI}_{0.99}Fe^{III}_{0.26}\square_{0.75})O_{4.75}(OH)_{1.5}$-

Always consult and cite the final, published document. See http:/www.minsocam.org or GeoscienceWorld

This is the peer-reviewed, final accepted version for American Mineralogist, published by the Mineralogical Society of America.
The published version is subject to change. Cite as Authors (Year) Title. American Mineralogist, in press.
DOI: https://doi.org/10.2138/am-2022-8112. http://www.minsocam.org/

$(H_2O)_{1.75}](H_2O)_{1.67}$ (H_2O from the stochiometry derived by the structure determination), demonstrates that it is Ba-dominant, with some variations in the Ba:Pb ratio. The studied aggregates from the type specimen contain neither K nor Bi. The IMA formula, which considers the mineral as Fe^{2+}-dominant, should therefore be revised entirely.

IMPLICATIONS

In contrast to schoepite-related minerals and phases formed during the initial stages of uraninite alteration, uranotungstite belongs to the group of supergene phases derived from the long-term alteration of uraninite, similarly to, e.g., the uranyl-oxide mineral uranosphaerite, $Bi(UO_2)O_2(OH)$ (Hughes et al. 2003; Plášil 2018; Colmenero et al. 2020). Those uranyl-oxide minerals that belong to the long-term alteration products are characteristic concerning their high molar proportion of incorporated metal elements by comparison to the content of molecular H_2O in their crystal structures (Finch and Ewing 1992; Plášil 2018). These metal elements are usually released from the gradually weathering uraninite (such as radiogenic Pb) and host rocks (Na, K, Ca). In the case of uranotungstite, the molar proportion of metal cations to molecular H_2O is 0.31:0.43 (from crystal-structure data) and the molar *Me*:U ratio is 0.31:0.26, thus matching the region of "relic" phases (*cf.* Plášil 2018).

Among others, we have investigated "uranotungstite" specimens from the Medvědín uranium deposit that enabled a more detailed look at the mineral association at the micro-scale. A uranotungstite-like mineral (containing Bi dominating over Pb) from Medvědín belongs undoubtedly to the "relic" phases. This conclusion is supported by the mineral assemblage (Fig. 7a) comprising uranophane-α (forming pseudomorphs after pitchblende and tiny veins), tabular crystals of saléeite and torbernite, and their relics, U-bearing to U-rich bismutoferrite, and,

Always consult and cite the final, published document. See http:/www.minsocam.org or GeoscienceWorld

This is the peer-reviewed, final accepted version for American Mineralogist, published by the Mineralogical Society of America.
The published version is subject to change. Cite as Authors (Year) Title. American Mineralogist, in press.
DOI: https://doi.org/10.2138/am-2022-8112. http://www.minsocam.org/

additionally, the Bi-dominant uranotungstite-like mineral. The latter forms relatively compact aggregates, to 10 μm across, embedded in the relics of torbernite and saléeite (Fig. 7b).

The high chemical variability and potentially close structural relationship of a large number of related Ba/Pb/Fe/W/Bi-substituted "uranotungstite-like" structures, which remain unclear at the moment, prompted further research into the mineralogy of weathered U(Bi/W)-deposits. We are convinced that such research can be important due to implications for nuclear waste management as Bi was a very common element used during the production of Pu since the 1940s.

ACKNOWLEDGMENTS

Comments by Travis Olds, an anonymous reviewer, and the structure editor helped us to significantly improve the manuscript. We are indebted to Stephan Wolfsried (Stuttgart, Germany), Carsten Slotta (Hausach, Germany), Dietmar Schrenk (Hornberg, Germany), Richard Bayerl (Stuttgart, Germany), and Heinz Förch (Sindelfingen, Germany) for providing us with samples for study. This work was financially supported by the Czech Science Foundation (GACR 20-11949S), by OP VVV project (Geobarr CZ.02.1.01/0.0/0.0/16_026/0008459 to RS), and the fieldwork at the Medvědín hill has been allowed by the Administration of the Krkonoše Mountains National Park.

REFERENCES

Atencio, D., Andrade, M.B., Christy, A.G., Gieré, R., and Kartashov, P.M. (2010) The pyrochlore supergroup of minerals: nomenclature. Canadian Mineralogist, 48, 673–698.

Brown, I.D. (1981) The bond-valence method: an empirical approach to chemical structure and bonding. In M. O'Keeffe and A. Navrotsky, Eds., Structure and Bonding in Crystals II.

Always consult and cite the final, published document. See http:/www.minsocam.org or GeoscienceWorld

This is the peer-reviewed, final accepted version for American Mineralogist, published by the Mineralogical Society of America.
The published version is subject to change. Cite as Authors (Year) Title. American Mineralogist, in press.
DOI: https://doi.org/10.2138/am-2022-8112. http://www.minsocam.org/

Academic Press, New York, 1–30.

Brown, I.D. (2002) The chemical bond in inorganic chemistry: the bond valence model. Oxford University Press, UK, 1–278.

Brugger, J., Krivovichev, S.V., Berlepsh, P., Meisser, N., Ansermet, S., and Armbruster, T. (2004) Spriggite, $Pb_3[(UO_2)_6O_8(OH)_2](H_2O)_3$, a new mineral with β-$U_3O_8$-type sheets: description and crystal structure. American Mineralogist, 89, 339–347.

Burns, P.C. (2005) U^{6+} minerals and inorganic compounds: insights into an expanded structural hierarchy of crystal structures. Canadian Mineralogist, 43, 1839–1894.

Burns, P.C., Ewing, R.C., and Hawthorne, F.C. (1997a) The crystal chemistry of hexavalent uranium: polyhedron geometries, bond-valence parameters, and polymerization of polyhedra. Canadian Mineralogist, 35, 1551–1570.

Burns, P.C., Finch, R.J., Hawthorne, F.C., Miller, M.L., and Ewing, R.C. (1997b) The crystal structure of ianthinite, $[U^{4+}_2(UO_2)_4O_6(OH)_4(H_2O)_4](H_2O)_5$: a possible phase for Pu^{4+} incorporation during the oxidation of spent nuclear fuel. Journal of Nuclear Materials, 24, 199–206.

Clabbers, M. T. B., Gruene, T., van Genderen, E., and Abrahams, J. P. (2019) Reducing dynamical electron scattering reveals hydrogen atoms. Acta Crystallographica A, 75, 82–93.

Colmenero, F., Plášil, J., and Němec, I. (2020) Uranosphaerite: Crystal structure, hydrogen bonding, mechanics, infrared and Raman spectroscopy and thermodynamics. J. Physics and Chemistry of Solids, 141, 109400.

Cuchet, S., Brugger, J., Meisser, N., Ansermet, S., and Chiappero, P.-J. (2000) Les minéraux du filon Sainte-Barbe, Les Montmins, Allier. Le Règne Minéral (33), 5–25 (in French).

Always consult and cite the final, published document. See http:/www.minsocam.org or GeoscienceWorld

This is the peer-reviewed, final accepted version for American Mineralogist, published by the Mineralogical Society of America.
The published version is subject to change. Cite as Authors (Year) Title. American Mineralogist, in press.
DOI: https://doi.org/10.2138/am-2022-8112. http://www.minsocam.org/

Evans, H.T., Jr. (1963) Uranyl ion coordination. Science, 141, 154–157.

Finch, R.J., and Ewing, R.C. (1992) The corrosion of uraninite under oxidizing conditions. Journal of Nuclear Materials, 190, 133–156.

Finch, R.J., and Murakami, T. (1999) Systematics and paragenesis of uranium minerals. In: Burns, P.C., Finch, R.J. (eds) Uranium: Mineralogy, Geochemistry and the Environment. Mineralogical Society of America and Geochemical Society Reviews in Mineralogy and Geochemistry, 38, pp 91–180.

Finch, R.J., Burns, P.C., Hawthorne, F.C., and Ewing, RC (2006) Refinement of the crystal structure of billietite $Ba[(UO_2)_6O_4(OH)_6](H_2O)_8$. Canadian Mineralogist, 44, 1197–1205.

Gagné, O.C., and Hawthorne, F.C. (2015) Comprehensive derivation of bond-valence parameters for ion pairs involving oxygen. Acta Crystallographica, B71, 562–578.

Gemmi, M., and Lanza, A. E. (2019) 3D electron diffraction techniques. Acta Crystallographica B, 75, 495–504.

Gemmi, M., Mugnaioli, E., Gorelik, T., Kolb, U., Palatinus, L., Boullay, P., Hovmöller, S., and Abrahams, J. (2019) 3D Electron Diffraction: The Nanocrystallography Revolution. ACS Central Science, 5, 1315–1329.

Janeczek, J., Ewing, R.C., Oversby, V.M., and Werme, L.O. (1996) Uraninite and UO_2 in spent nuclear fuel: a comparison. Journal of Nuclear Materials, 238, 121–130.

Kolb, U., Gorelik, T., Kübel, C., Otten, M. T., and Hubert, D. (2007) Towards automated diffraction tomography: Part I–Data acquisition. Ultramicroscopy, 107, 507–513.

Kolb, U., Gorelik, T., and Otten, M. T. (2008) Towards automated diffraction tomography. Part II–Cell parameter determination. Ultramicroscopy, 108, 763–772.

Always consult and cite the final, published document. See http:/www.minsocam.org or GeoscienceWorld

This is the peer-reviewed, final accepted version for American Mineralogist, published by the Mineralogical Society of America.
The published version is subject to change. Cite as Authors (Year) Title. American Mineralogist, in press.
DOI: https://doi.org/10.2138/am-2022-8112. http://www.minsocam.org/

Kolb, U., Krysiak, Y., and Plana-Ruiz, S. (2019) Automated electron diffraction tomography – development and applications. Acta Crystallographica B, 75, 463–474.

Krivovichev, S.V., and Plášil, J. (2013) Mineralogy and crystallography of uranium. In: Burns, P.C., Sigmon, G.E. (eds.) Uranium: From Cradle to Grave. Mineralogical Association of Canada Short Courses, 43, pp 15–119.

Loopstra, B.O. (1970) The structure of β-U_3O_8. Acta Crystallographica B, 26, 656–657.

Lussier, A.J., Lopez, R.A.K., and Burns, P.C. (2016) A revised and expanded structure hierarchy of natural and synthetic hexavalent uranium compounds. Canadian Mineralogist, 54, 177–283.

Miller, M.L., Finch, R.J., Burns, P.C., and Ewing, R.C. (1996) Description and classification of uranium oxide hydrate sheet anion topologies. Journal of Materials Research, 11, 3048–3056.

Mugnaioli, E., Gorelik, T., and Kolb, U. (2009) "Ab–initio" structure solution from electron diffraction data obtained by a combination of automated diffraction tomography and precession technique. Ultramicroscopy, 109, 758–765.

Mugnaioli, E., Lanza, A. E., Bortolozzi, G., Righi, L., Merlini, M., Cappello, V., Marini, L., Athanassiou, A., and Gemmi, M. (2020) Electron Diffraction on Flash-Frozen Cowlesite Reveals the Structure of the First Two-Dimensional Natural Zeolite. ACS Central Science, **6**, 1578–1586.

Olds, T.A., Lussier, A.J., Oliver, A.G., Petříček, V., Plášil, J., Kampf, A.R., Burns, P.C., Dembowski, M., Carlson, S.M., and Steele, I.M. (2017) Shinkolobweite, IMA 2016-095. CNMNC Newsletter No. 36, April 2017, page 404; Mineralogical Magazine, 81, 403–409.

Always consult and cite the final, published document. See http:/www.minsocam.org or GeoscienceWorld

Palatinus, L. (2013) The charge-flipping algorithm in crystallography. Acta Crystallographica B, 69, 1–16.

Palatinus, L., and Chapuis, G. (2007) SUPERFLIP – a computer program for the solution of crystal structures by charge flipping in arbitrary dimensions. Journal of Applied Crystallography, 40, 786–790.

Palatinus, L., Brázda, P., Boullay, P., Perez, O., Klementová, M., Petit, S., Eigner, V., Zaarour, M., and Mintova, S. (2017) Hydrogen positions in single nanocrystals revealed by electron diffraction. Science, 355, 166–169.

Palatinus, L., Brázda, P., Jelínek, M., Hrdá, J., Steciuk, G., and Klementová, M. (2019) Specifics of the data processing of precession electron diffraction tomography data and their implementation in the program PETS2.0. Acta Crystallographica B, 75, 512–522.

Petříček, V., Dušek, M., and Palatinus, L. (2014) Crystallographic computing system Jana2006: general features. Zeitschrift für Kristallographie, 229, 345–352.

Plana-Ruiz, S., Krysiak, Y., Portillo, J., Alig, E., Estradé, S., Peiró, F., and Kolb, U. (2020) Fast-ADT: A fast and automated electron diffraction tomography setup for structure determination and refinement. Ultramicroscopy, 211, 112951.

Plášil, J. (2014) Oxidation–hydration weathering of uraninite: the current state-of-knowledge. Journal of Geosciences, 59, 99–114.

Plášil, J. (2018) Uranyl-oxide hydroxy-hydrate minerals: their structural complexity and evolution trends. European Journal of Mineralogy, 30, 237–251.

Plášil, J., Sejkora, J., Čejka, J., Škoda, R., and Goliáš, V. (2009) Supergene mineralization of the Medvědín uranium deposit, Krkonoše Mountains, Czech Republic. Journal of Geosciences,

Always consult and cite the final, published document. See http:/www.minsocam.org or GeoscienceWorld

This is the peer-reviewed, final accepted version for American Mineralogist, published by the Mineralogical Society of America.
The published version is subject to change. Cite as Authors (Year) Title. American Mineralogist, in press.
DOI: https://doi.org/10.2138/am-2022-8112. http://www.minsocam.org/

54, 15–56.

Plášil, J., Škoda, R., Čejka, J., Bourgoin, V., and Boulliard, J.-C. (2016) Crystal structure of the uranyl-oxide mineral rameauite. European Journal of Mineralogy, 28, 959–967.

Plášil, J., Kampf, A.R., Škoda, R., and Čejka, J. (2018) Nollmotzite, $Mg[U^{V}(U^{VI}O_2)_2O_4F_3]\cdot 4H_2O$, the first natural uranium oxide containing fluorine. Acta Crystallographica B, 74, 362–369.

Pouchou, J.L., and Pichoir, F. (1985) "PAP" (φρZ) procedure for improved quantitative microanalysis. In: Armstrong JT (ed) Microbeam Analysis. San Francisco Press, San Francisco, pp 104–106.

Steciuk, G., Ghazisaeed, S., Kiefer, B., and Plášil, J. (2019) Crystal structure of vyacheslavite, $U(PO_4)(OH)$, solved from natural nanocrystal: a precession electron diffraction tomography (PEDT) study and DFT calculations. RSC Advances, 9, 19657–19661.

Steciuk, G., Majzlan, J., and Plášil, J. (2021) Hydrogen disorder in kaatialaite $Fe[AsO_2(OH)_2].5H_2O$ from Jáchymov, Czech Republic: determination from low-temperature 3D electron diffraction. IUCrJ, 8, 2052–2525.

Steciuk, G., Škoda, R., Rohlíček, J., and Plášil, J. (2020) Crystal structure of the uranyl–molybdate mineral calcurmolite $Ca[(UO_2)_3(MoO_4)_2(OH)_4](H_2O)_{\sim 5.0}$: insights from a precession electron-diffraction tomography study. Journal of Geoscience, 65, 15–25.

Vincent, R., and Midgley, P.A. (1994) Double conical beam-rocking system for measurement of integrated electron diffraction intensities. Ultramicroscopy, 53, 271–282.

Walenta, K. (1985) Uranotungstit, ein neues sekundäres Uranmineral aus dem Schwarzwald. Tschermaks Mineralogische und Petrographische Mitteilungen, 34, 25–34 (in German).

Walenta, K. (1992) Die Mineralien des Schwarzwaldes. Chr. Weise Verlag, Munich, Germany,

Always consult and cite the final, published document. See http:/www.minsocam.org or GeoscienceWorld

This is the peer-reviewed, final accepted version for American Mineralogist, published by the Mineralogical Society of America.
The published version is subject to change. Cite as Authors (Year) Title. American Mineralogist, in press.
DOI: https://doi.org/10.2138/am-2022-8112. http://www.minsocam.org/

336 pp (in German).

Wronkiewicz, D.J., Bates, J.K., Gerding, T.J., and Veleckis, E. (1992) Uranium release and secondary phase formation during unsaturated testing of UO_2 at 90 °C. Journal of Nuclear Materials, 190, 107–127.

Wronkiewicz, D.J., Bates, J.K., Wolf, S.F., and Bick, E.C. (1996) Ten-year results from unsaturated drip tests with UO_2 at 90 °C: implications for the corrosion of spent nuclear fuel. Journal of Nuclear Materials, 238, 78–95.

Always consult and cite the final, published document. See http:/www.minsocam.org or GeoscienceWorld

This is the peer-reviewed, final accepted version for American Mineralogist, published by the Mineralogical Society of America.
The published version is subject to change. Cite as Authors (Year) Title. American Mineralogist, in press.
DOI: https://doi.org/10.2138/am-2022-8112. http://www.minsocam.org/

FIGURE CAPTIONS

FIGURE 1 Uranotungstite (orange spherules) from Menzenschwand uranium deposit used for PEDT experiment (sample 2). Associated are uranophane-α (as very thin prismatic crystals) in a vug of quartz-dominant gangue (smoky quartz to dark amethyst). Field of view 2 mm, photographed by Pavel Škácha.

FIGURE 2 EDS spectrum of one of the uranotungstite fragments used for the structure determination by 3D electron diffraction techniques. Major Cu peak is due to copper-grid used for sample deposition.

FIGURE 3. Left: Uranotungstite crystals selected for the 3D ED data among the accompanying francevillite crystals. Right: Two sections, *h*0*l* and *hk*0, of the reciprocal space reconstructed in PETS2 (Palatinus et al. 2019).

FIGURE 4. a) Possible local conformations A, B, C, and D of the uranotungstite structure due to the cationic disorder and b) a corresponding number of *x* (blue) and *n theoretical* (grey) hydroxyl and water molecules allowed by each local conformation. *x* is the number of $OH+H_2O$ visible in the refined model, *n* is the theoretical number of additional water molecules in the interlayer.

FIGURE 5. Structural sheets in uranotungstite of the β-U_3O_8 type: a) uranyl-tungstate sheet perpendicular to **c** (color scheme same as in the previous figure); unit-cell edges are outlined in black solid lines; b) graph representation of the topology; c) corresponding chains: D – pentagons with triangles oriented down, R – rectangles; U – pentagons with triangles oriented up.

FIGURE 6. Crystal structure of uranotungstite viewed down the monoclinic *b*-axis. Color scheme: UO_7 polyhedra yellow, $(W,Fe)O_5$ polyhedra green, Ba/Pb-O polyhedra light green, O atoms red, H atoms light grey; unit-cell edges outlined in black solid lines.

FIGURE 7. Uranotungstite from Medvědín BSE images of a polished sample). **a)** Entire mineral assemblage including uranophane (Urp-α) replacing pitchblende, U-bearing to U-rich bismutoferrite (Bif). The rest of the matrix comprises relics of probable uranyl micas: saléeite and torbernite. Utgs – uranotungstite. **b)** Detailed view of the area marked with a red square in a). Spherules of uranotungstite (Utgs) are embedded in torbernite (Tor) and saléeite (Slé) relics. The rim of a veinlet formed by saléeite is formed by U-bearing bismutoferrite (Bif).

Always consult and cite the final, published document. See http:/www.minsocam.org or GeoscienceWorld

This is the peer-reviewed, final accepted version for American Mineralogist, published by the Mineralogical Society of America.
The published version is subject to change. Cite as Authors (Year) Title. American Mineralogist, in press.
DOI: https://doi.org/10.2138/am-2022-8112. http://www.minsocam.org/

Tables

Table 1. Chemical composition (in wt.% oxides, from EPMA) of the holotype specimen of uranotungstite from Menzenschwand.

Constituent	Mean	Range	Stand. Dev.	Standard
PbO	5.49	5.30–5.80	0.19	vanadinite
BaO	4.76	4.54–5.02	0.15	baryte
FeO	1.67	1.55–1.73	0.06	andradite
WO_3	20.65	19.87–22.04	0.72	syn. $ZnWO_4$
UO_3	51.35	50.63–53.65	1.07	parsonsite
Total	83.96			

Table 2. Selected bond distances (Å) for uranotungstite.

U–O		W1/Fe1–O		O–H	
U1–O2	1.797(12)	W1/Fe1–O3	2.25(2)	O3–H1O3	1.00(2)
U1–O7	2.404(7)	W1/Fe1–O4	1.898(5)	O3–H2O3	0.997(17)
U1–O7	2.404(7)	W1/Fe1–O5	1.894(13)		
U1–O8	1.793(12)	W1/Fe1–O7	1.919(7)	H···O (H···*A*)	
U1–O9	2.287(6)	W1/Fe1–O9	1.875(6)	H1O3···O1	1.96(2)
U1–O9	2.287(6)	W1/Fe1–O11	1.910(5)	H2O3···O2	1.947(16)
U1–O11	2.387(9)				
		Ba1/Pb1–O			
U2–O1	1.802(12)	Ba1/Pb1–O5	2.711(13)		
U2–O4	2.446(9)	Ba1/Pb1–O5	2.735 (13)		
U2–O6	1.790(12)	Ba1/Pb1–O5	2.735(13)		
U2–O7	2.197(6)	Ba1/Pb1–O5	2.711(13)		
U2–O7	2.197(6)	Ba1/Pb1–O6	2.856(15)		
U2–O9	2.343(7)	Ba1/Pb1–O8	2.862(15)		
U2–O9	2.343(7)	Ba1/Pb1–O10	2.60(2)		
		Ba1/Pb1–O10	2.60(2)		

Always consult and cite the final, published document. See http:/www.minsocam.org or GeoscienceWorld

This is the peer-reviewed, final accepted version for American Mineralogist, published by the Mineralogical Society of America.
The published version is subject to change. Cite as Authors (Year) Title. American Mineralogist, in press.
DOI: https://doi.org/10.2138/am-2022-8112. http://www.minsocam.org/

1

Always consult and cite the final, published document. See http:/www.minsocam.org or GeoscienceWorld

This is the peer-reviewed, final accepted version for American Mineralogist, published by the Mineralogical Society of America.
The published version is subject to change. Cite as Authors (Year) Title. American Mineralogist, in press.
DOI: https://doi.org/10.2138/am-2022-8112. http://www.minsocam.org/

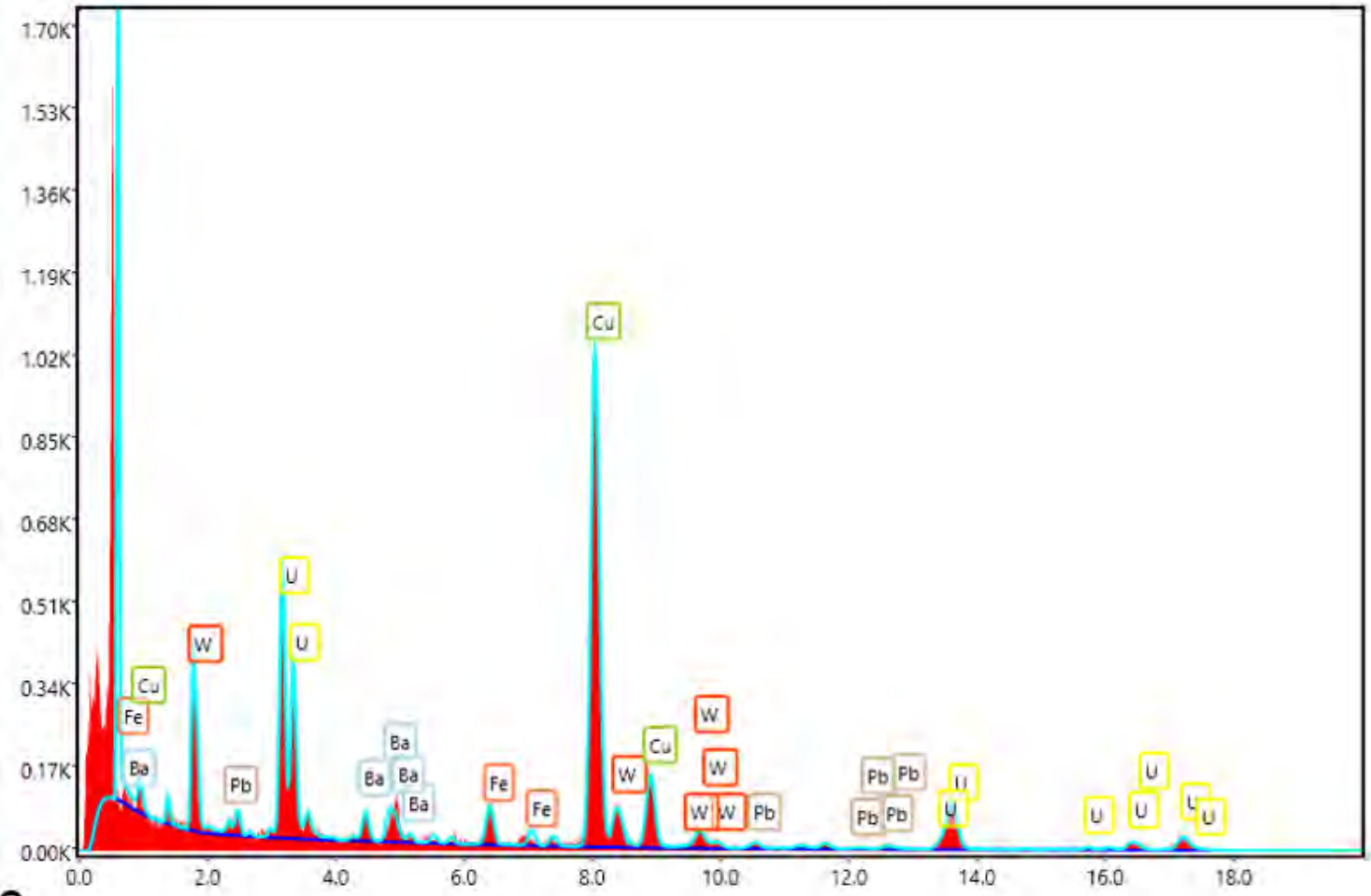

2

Always consult and cite the final, published document. See http:/www.minsocam.org or GeoscienceWorld

This is the peer-reviewed, final accepted version for American Mineralogist, published by the Mineralogical Society of America.
The published version is subject to change. Cite as Authors (Year) Title. American Mineralogist, in press.
DOI: https://doi.org/10.2138/am-2022-8112. http://www.minsocam.org/

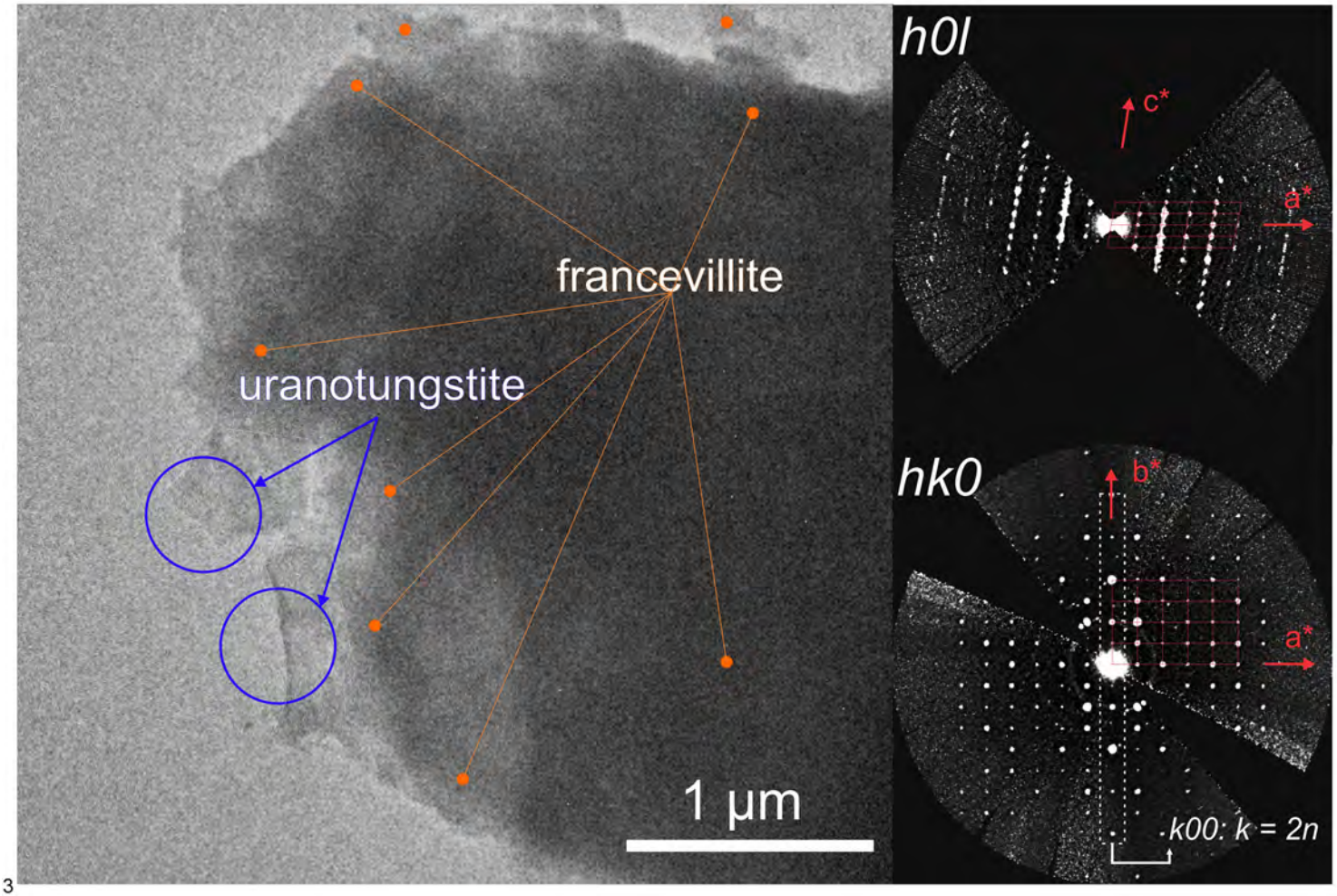

3

Always consult and cite the final, published document. See http:/www.minsocam.org or GeoscienceWorld

This is the peer-reviewed, final accepted version for American Mineralogist, published by the Mineralogical Society of America.
The published version is subject to change. Cite as Authors (Year) Title. American Mineralogist, in press.
DOI: https://doi.org/10.2138/am-2022-8112. http://www.minsocam.org/

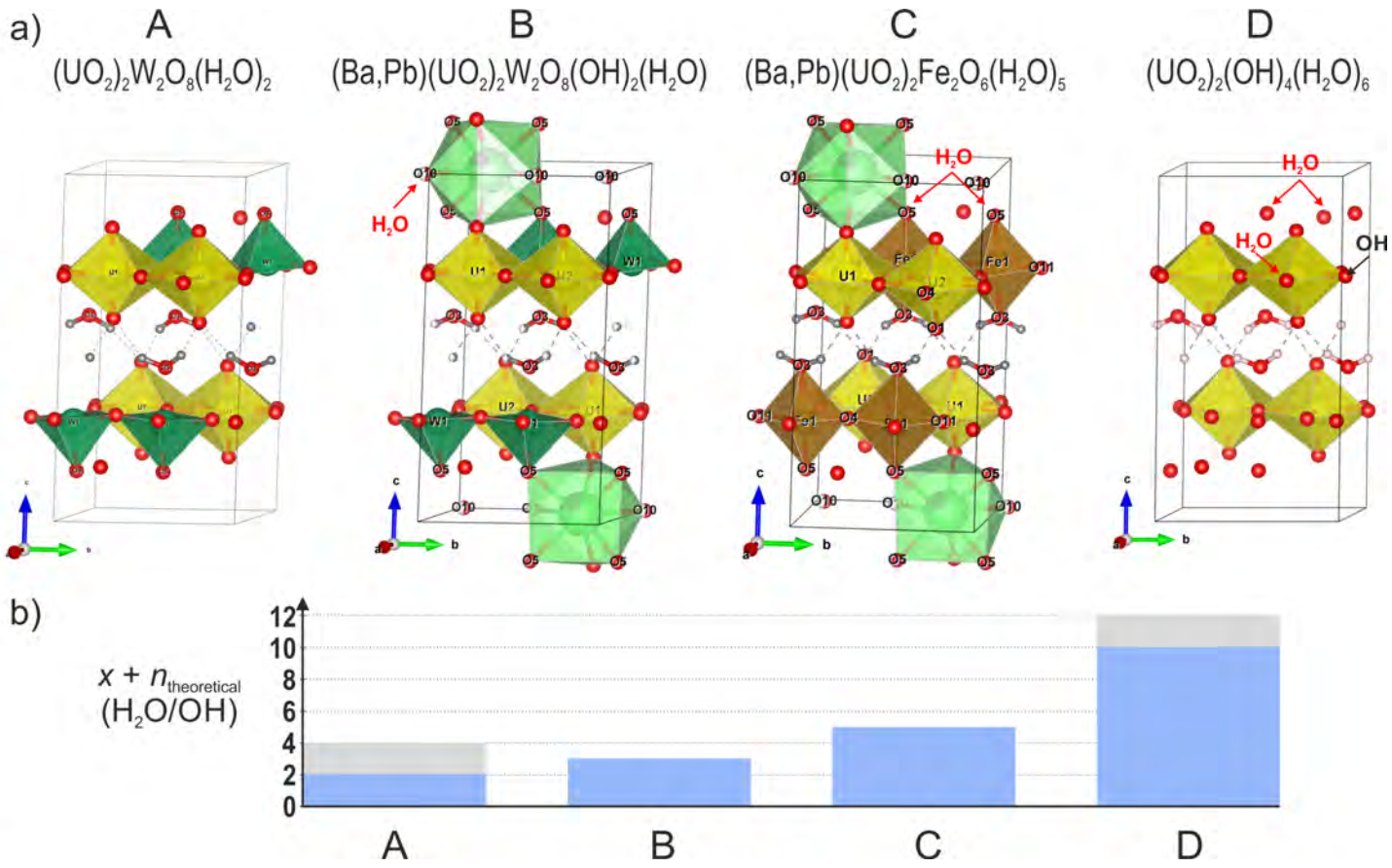

Always consult and cite the final, published document. See http:/www.minsocam.org or GeoscienceWorld

This is the peer-reviewed, final accepted version for American Mineralogist, published by the Mineralogical Society of America.
The published version is subject to change. Cite as Authors (Year) Title. American Mineralogist, in press.
DOI: https://doi.org/10.2138/am-2022-8112. http://www.minsocam.org/

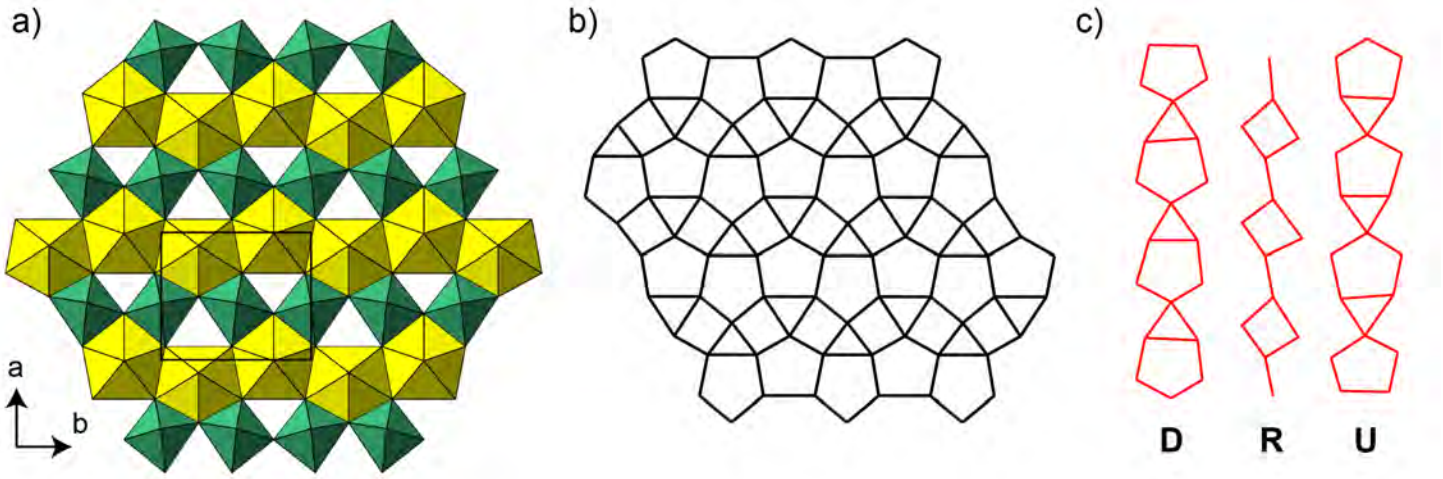

5

Always consult and cite the final, published document. See http:/www.minsocam.org or GeoscienceWorld

This is the peer-reviewed, final accepted version for American Mineralogist, published by the Mineralogical Society of America.
The published version is subject to change. Cite as Authors (Year) Title. American Mineralogist, in press.
DOI: https://doi.org/10.2138/am-2022-8112. http://www.minsocam.org/

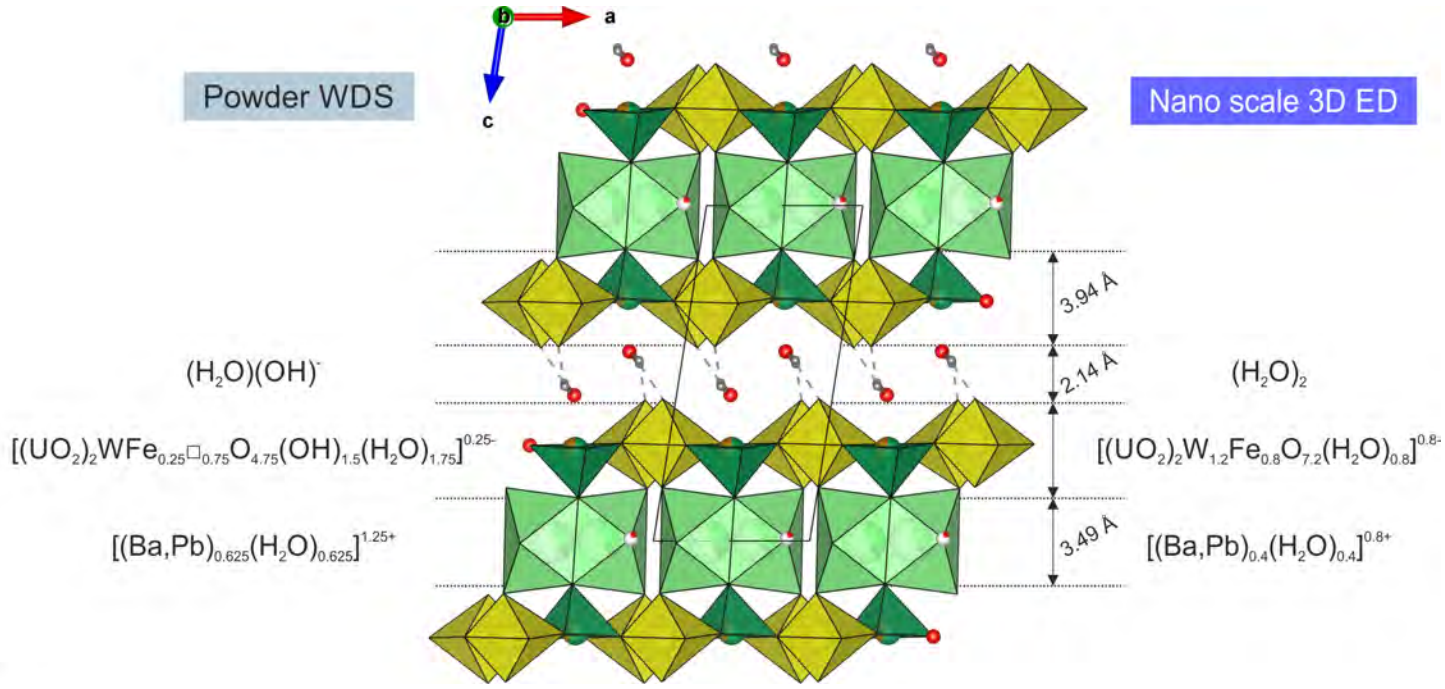

Always consult and cite the final, published document. See http:/www.minsocam.org or GeoscienceWorld

This is the peer-reviewed, final accepted version for American Mineralogist, published by the Mineralogical Society of America.
The published version is subject to change. Cite as Authors (Year) Title. American Mineralogist, in press.
DOI: https://doi.org/10.2138/am-2022-8112. http://www.minsocam.org/

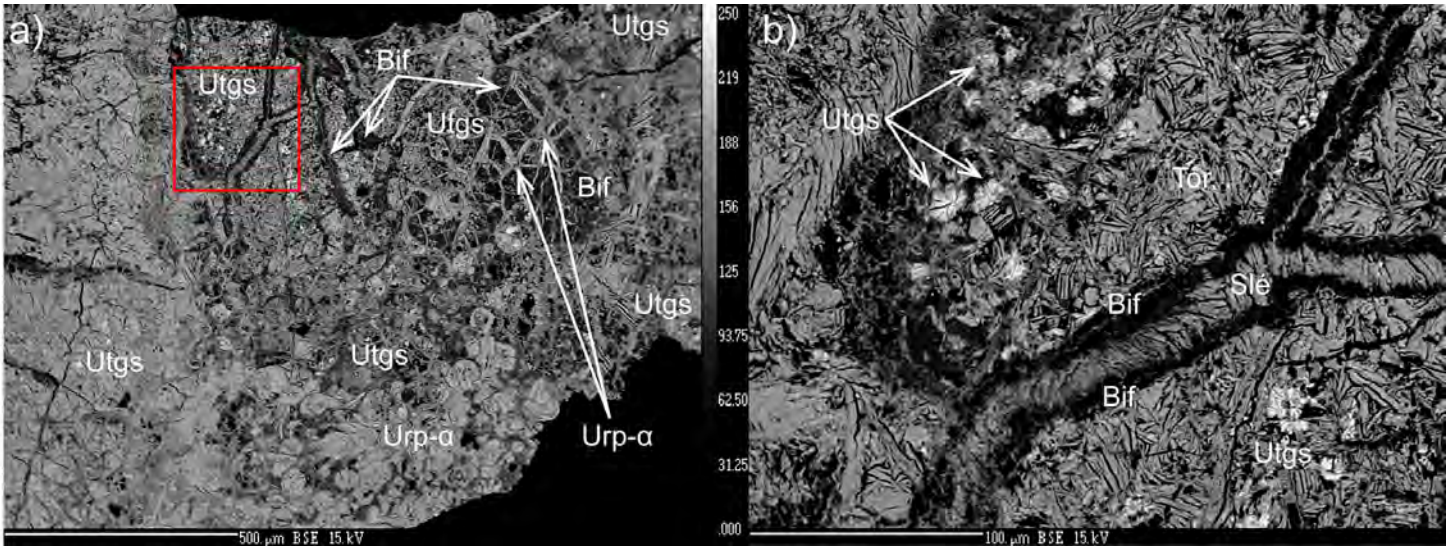

Always consult and cite the final, published document. See http:/www.minsocam.org or GeoscienceWorld